



PRIFYSGOL  
**BANGOR**  
UNIVERSITY

## Tides on Other Earths: Implications for Exoplanet and Palaeo-Tidal Simulations

Blackledge, Benedict; Green, Mattias; Barnes, Rory ; Way, Michael

### Geophysical Research Letters

DOI:

[10.1029/2019GL085746](https://doi.org/10.1029/2019GL085746)

Published: 28/06/2020

Peer reviewed version

[Cyswllt i'r cyhoeddiad / Link to publication](#)

*Dyfyniad o'r fersiwn a gyhoeddwyd / Citation for published version (APA):*

Blackledge, B., Green, M., Barnes, R., & Way, M. (2020). Tides on Other Earths: Implications for Exoplanet and Palaeo-Tidal Simulations. *Geophysical Research Letters*, 47(12), [e2019GL085746]. <https://doi.org/10.1029/2019GL085746>

#### Hawliau Cyffredinol / General rights

Copyright and moral rights for the publications made accessible in the public portal are retained by the authors and/or other copyright owners and it is a condition of accessing publications that users recognise and abide by the legal requirements associated with these rights.

- Users may download and print one copy of any publication from the public portal for the purpose of private study or research.
- You may not further distribute the material or use it for any profit-making activity or commercial gain
- You may freely distribute the URL identifying the publication in the public portal ?

#### Take down policy

If you believe that this document breaches copyright please contact us providing details, and we will remove access to the work immediately and investigate your claim.

# Tides on other Earths: implications for exoplanet and palaeo-tidal simulations

B. W. Blackledge<sup>1</sup>, J. A. M. Green<sup>1</sup>, R. Barnes<sup>2</sup>, and M. J. Way<sup>3,4,5</sup>

<sup>1</sup>School of Ocean Sciences, Bangor University, Menai Bridge, UK

<sup>2</sup>Department of Astronomy, University of Washington, Seattle, Wa, USA

<sup>3</sup>NASA Goddard Institute for Space Studies, New York, USA

<sup>4</sup>Goddard Space Flight Center Sellers Exoplanet Environments Collaboration

<sup>5</sup>Theoretical Astrophysics, Department of Physics and Astronomy, Uppsala University, Uppsala, Sweden

## Key Points:

- The possible tidal dissipation rates on Earth can span at least 3 orders of magnitude, with bathymetry this range narrows.
- Geologic features currently unique to Earth are crucial factors in the tidal energy budget.
- Time varying dissipation due to surface evolution such as tectonics should be considered in models of evolving planetary rotation.

---

Corresponding author: Dr J. A. M. Green, [m.green@bangor.ac.uk](mailto:m.green@bangor.ac.uk)

**Abstract**

A key controller of a planet’s rotational evolution, and hence habitability, is tidal dissipation, which on Earth is dominated by the ocean tides. Because exoplanet or deep-time Earth topographies are unknown, a statistical ensemble is used to constrain possible tidal dissipation rates on Earth and similar ecoplanets. A dedicated tidal model is used together with 120 random continental configurations to simulate Earth’s semi-diurnal lunar tide. The results show a possible ocean tidal dissipation range spanning 3 orders of magnitude, between 2.3GW–1.9TW (1TW=10<sup>12</sup>W). When model resolution is considered, this compares well with theoretical limits derived for the energetics of Earth’s present day deep-ocean-only environment. Consequently, continents exert a fundamental control on tidal dissipation rates and we suggest that if plate tectonics are present on a planet it will induce a time-varying dissipation analogous to Earth’s. This will alter rotational periods over millions of years and further complicate the role of tides for planetary evolution.

**Plain Language Summary**

The daylength of a planet is key for habitability because it regulates the rate with which solar radiation is received and redistributed at the surface. A main controller of a planet’s daylength is the ocean tide, because the dissipation of tidal energy works as a brake on the planet’s spin, increasing the daylength. Tides are sensitive to the continental arrangement on a planet, but there are no details of the surface of any exoplanet and only limited information of what Earth looked like in the distant past. The change in Earth’s daylength forces the Moon to recede into a higher orbit, but the present-day recession rate is very high and doesn’t fit our age models of the moon, implying the tides must have been much weaker in the distant past. Here, we use a series of tidal predictions for random continental configurations of Earth to provide a range of tidal dissipation rates and thus an estimate of how the tides in the deep past may have evolved as Earth’s continents grew more and more complex. This research also provides a range of dissipation rates that can be used for simulations of the rotational and orbital evolution of exoplanets.

**1 Introduction**

The ocean tides drive and influence a range of geophysical processes. The tidal energy dissipated in shallow waters controls shelf sea stratification (Simpson et al., 1990) and sustains a vertical nutrient flux vital for marine primary productivity in shallow and deep environments (Hickman et al., 2012; Williams et al., 2018; Tuerena et al., 2019). In the deep ocean, tidally driven mixing is integral to the global overturning circulation (Kuhlbrodt et al., 2007; Srokosz et al., 2012; Wunsch & Ferrari, 2004), whereas the tidal range during particular geologic periods may exert an influence on the evolution of complex life (Balbus, 2014). The tides are also a first-order control on orbital evolution for the Earth-Moon system (Bills & Ray, 1999; Munk, 1968). This is illustrated through the current, anomalously high, (3.8cm yr<sup>-1</sup>) recession rate of the Moon which does not match its radiometric age of 4.5 Gyr (Dickey et al., 1994; Barnes, 2017). The erroneous assumption of a constant modern globally integrated dissipation rate suggests an Earth-Moon system age of about 1.5 Gyr (Darwin, 1899; MacDonald, 1964; Munk, 1968). The missing factor may be the time-varying effect of the continental configuration on the tide, a condition shown to have driven long-term dissipation variability on Earth (Kagan, 1997; Green et al., 2017). Consequently, the implications of an ocean tide controlled by a planets’ continental configuration is an important parameter when modelling the orbital evolution of an ocean bearing planet.

To date, there are over 4000 confirmed exoplanets, of which more than 630 are in multi-planet systems (see <http://exoplanet.eu/catalog/> for the latest estimate). The masses

66 of these planets range from gas giants of the order of  $\sim 1000 M_{\oplus}$  (Earth masses), to less  
 67 massive objects that are often characterised as terrestrial planets, thought to be simi-  
 68 lar in composition and scale to the terrestrial planets in our solar system (exoplanets.eu).  
 69 Concurrently, attempts have been made to estimate the ‘habitability’ of these planets,  
 70 a condition based on the probability of a given planet being able to support liquid wa-  
 71 ter at its surface (Kasting et al., 1993) – one of many definitions for habitability. This  
 72 is a function of host star irradiance, planet-star separation and the chemical composi-  
 73 tion of the planet and its climate system (Seager, 2013). These conditions determine the  
 74 extent of the Habitable Zone, the theoretical shell around a given star at which liquid  
 75 water could exist, given the appropriate climatic conditions (Kopparapu et al., 2013).

76 As the number of confirmed planets has grown, planets with potential oceans emerge  
 77 (e.g., Tsiaras et al., 2019), and the number of planets that appear to be within their hab-  
 78 itable zone is expected to increase (Batalha et al., 2013). Estimates put the number of  
 79 planets in the Milky Way as high as  $\sim 10^{10}$  (Dressing & Charbonneau, 2015). Since smaller,  
 80 potentially terrestrial, planets far outnumber the larger gaseous planets (Cassan et al.,  
 81 2012; Howard, 2013; Fressin et al., 2013), habitable planets may be common.

82 Little is known about these planets, which has led to the widespread use of numer-  
 83 ical models of potential climatic conditions to determine a probability of a given body  
 84 hosting water (Seager, 2013), but there are large uncertainties in this approach. For ex-  
 85 ample, varying host-star irradiances and masses, and planetary atmospheric composi-  
 86 tions, masses, rotation rates, eccentricities, and obliquities will drastically alter the con-  
 87 ditions at the surface (Kasting et al., 1993; Williams & Pollard, 2002, 2003; Yang et al.,  
 88 2014; Way et al., 2016; Way & Georgakarakos, 2017; Way et al., 2018; Colose et al., 2019).  
 89 Few of these simulations, however, consider the effect of a water ocean tide, despite tidal  
 90 friction being a key controller on orbital evolution, and hence habitability (Bills & Ray,  
 91 1999; Lingam & Loeb, 2018; Egbert et al., 2004; Green et al., 2019).

92 If a planet’s spin frequency is greater than its moon’s orbital frequency, tidal fric-  
 93 tion will increase the semi-major axis length and rotational period of the planet, lead-  
 94 ing to a transfer of angular momentum due to the torques exerted on the body (Darwin,  
 95 1899). This process leads to an increase of the angular momentum of the tide raiser and  
 96 a decrease in the planet’s rotation rate, so the rotational evolution depends on the amount  
 97 of tidal energy dissipation. This is in turn a function of the height of the tidal bulges and  
 98 the rheology of the planet’s interior (Renaud & Henning, 2017), including the fraction  
 99 of water on it. On Earth today, the solid body dissipation for the dominating  $M_2$  lunar  
 100 tide is 0.08TW (Ray et al., 1996), whereas the associated total ocean tidal dissipation  
 101 rate is 2.4TW (Egbert & Ray, 2001). Obviously, a liquid ocean can provide a more en-  
 102 ergetic tidal response than a solid body alone because it is easier to excite a tide in the  
 103 ocean than in the solid Earth.

104 There are links between a planet’s potential habitability and its rotation rate, e.g.,  
 105 full spin-orbit synchronization at lower rates and the reduction of meridional atmospheric  
 106 convection at higher rotation rates due to a stronger Coriolis force (Yang et al., 2014).  
 107 To properly constrain a planet’s climatology, and therefore habitability, a range of vari-  
 108 ables, including the rotation rate, topography and land/ocean mask, must be known (Yang  
 109 et al., 2014; Way et al., 2016; Way & Del Genio, 2019; Colose et al., 2019). So a planet’s  
 110 past, present and future total tidal dissipation rate must be quantified, to improve es-  
 111 timates of those other dependent properties.

112 Here, we constrain the potential range of tidal dissipation on an Earth-like planet  
 113 using a dedicated numerical tidal model and a large sample of random continental con-  
 114 figurations. This will allow us to produce bounds on the potential dissipation rates that  
 115 can then be used for rotational evolution simulations, and to provide error bounds on  
 116 simulations of deep-time tides when Earth’s surface looked very different from today’s.

## 2 Methods

We use OTIS, the Oregon State University Tidal Inversion Software, a well established numerical tidal model that has been used to simulate deep-time past, present and future tides on Earth (Egbert et al., 2004; Green et al., 2017, 2018; Wilmes et al., 2017), and on ancient Venus (Green et al., 2019). The model has been bench-marked against other global non-assimilating tidal models and demonstrated to reproduce Earth's present day tide with a high degree of accuracy (Stammer et al., 2014). It solves the linearised shallow-water equations,

$$\frac{\partial \mathbf{U}}{\partial t} + \mathbf{f} \times \mathbf{U} = -gH\nabla(\eta - \eta_{EQ} - \eta_{SAL}) - \mathbf{F}, \quad (1)$$

$$\frac{\partial \eta}{\partial t} = -\nabla \cdot \mathbf{U} \quad (2)$$

where  $\mathbf{U}$  is the depth integrated volume transport (the current velocity  $u$  times the depth  $H$ ),  $g$  is the gravitational constant,  $\mathbf{f}$  the Coriolis vector,  $\zeta$  is the tidal amplitude.  $\eta_{SAL}$  is the elevation due to self-attraction and loading (SAL; here set to 8% of the amplitude following Ray (1997)) and  $\eta_{EQ}$  the equilibrium tidal elevation. The model is forced by the astronomical tide generated by the Lunar and Solar gravitational potential.  $\mathbf{F} = \mathbf{F}_B + \mathbf{F}_w$  is the total loss of energy to bed friction ( $F_B$ ) and tidal conversion ( $F_w$ , describing the generation of an internal tide). The scalar product  $\mathbf{F} \cdot \mathbf{u}$  thus gives the tidal dissipation rate,  $D$ . Bed friction is given by

$$\mathbf{F}_B = C_d \mathbf{u} |\mathbf{u}| \quad (3)$$

The drag coefficient,  $C_d=0.003$ , represents mean seabed roughness and is based on an appropriate value for present day Earth (see, e.g., Taylor, 1920), and  $\mathbf{u}$  is the combined velocity vector of all the tidal constituents. Note that the model is insensitive to the chosen value of  $C_d$ , and sensitivity simulations (not shown) with it varying by a factor 3 did not significantly change the results. However, this may not be the case for aqua-planets (no continents), where the dissipation may scale directly with  $C_d$  due to a lack of topography. Furthermore, for Earth-like ocean with fine sediments we do not expect  $C_d$  to vary beyond this parameter range.

Tidal conversion is important in simulations with topography, and is given by  $F_w = C|\mathbf{U}|$ , where  $C$  is the conversion coefficient given by (Zaron & Egbert, 2006):

$$C(x, y) = \gamma \frac{(\nabla H)^2 N_b \bar{N}}{8\pi^2 \omega}. \quad (4)$$

Here,  $\gamma=50$  is a scaling factor,  $N_b$  is the buoyancy frequency at the seabed,  $\bar{N}$  is the average buoyancy frequency in the vertical, and  $\omega$  is the frequency of the constituent under investigation. Given the surface properties of exoplanets are unknown, the buoyancy frequency is computed from a statistical fit based on observations from present day Earth, or  $N(x, y) = 0.00524 \exp(-z/1300)$ , where  $z$  is the vertical coordinate, and the constants 0.00524 and 1300 have units of  $s^{-1}$  and m, respectively. Tidal conversion will differ for other fluids (ie: liquid Methane), but we assume a water ocean here.

All simulations were performed for three dominating tidal constituents, but we focus our discussion on those representing the principal semi-diurnal lunar ( $M_2$ ) and solar ( $S_2$ ) tides. Their respective constituent periods for Earth today are 12.42, 12 and 23.93 hours. Note that OTIS handles tides only; there is no other forcing included in the model and although inertial oscillations are present we only discuss the ocean tides here.

### 2.1 Continental configurations and sensitivity simulations

The model grids were generated using Planet Generator (<https://topps.diku.dk/torbenm/maps.msp>), a fractal map generator capable of simulating complex planet sur-

158 face features, which is feasible because the shape and distribution of continents are ap-  
 159 proximately fractal-like in nature (Goodchild & Mark, 1987; Mandelbrot, 1982). The gen-  
 160 erator produces grey-scale images, where each pixel value is between 1 (white) and 0 (black).  
 161 Here, the images were  $360 \times 180$  pixels in size, and a flat-bottomed 'bath-tub' ocean grid,  
 162 at a horizontal resolution of  $1^\circ \times 1^\circ$ , was built by allocating a depth of 4500 m to all  
 163 grey-scale pixels with a value below 0.2. The aim here is to evaluate the effect of the po-  
 164 sition and complexity of the continents on the tide, and a further series of sensitivity sim-  
 165 ulations on the boundary values was performed, with the coastline at grey-scale values  
 166 of 0.1 and 0.4, as well as simulations with bottom topography (see below).

167 In total, 120 different continental configurations were evaluated, including an equi-  
 168 librium tide simulation without continents (See Table in Supplementary Material for a  
 169 summary of all the simulations). As each configuration is unique, all configurations are  
 170 independent of one another, so their general geometry and relative positions are hetero-  
 171 geneous. This represents (to some degree) the variation that would be expected between  
 172 planets, and between geological epochs on the same planet. To show the total effect of  
 173 continent size, ocean basin size and coastal complexity, we use the non-dimensional value  
 174  $R = L_{tot}/\sqrt{A_{ocean}}$ .  $L_{tot}$  is the total coastline length (km) and  $A_{ocean}$  ( $\text{km}^2$ ) is the to-  
 175 tal ocean area.  $L_{tot}$  was found by identifying the coordinates of the coastal boundary  
 176 between individual continents and the ocean. The distance between neighbouring coordi-  
 177 nates were then calculated using a Great-circle technique: the coastal length for each  
 178 continent was found, and the total global distance was the sum of these values. This is  
 179 justified as there is little point considering distances smaller than the smallest horizon-  
 180 tal resolution in the grid, although Earths' real tides are influenced by small, non-random  
 181 topographic features.

182 We also completed two sets of simulations with ocean bathymetry for 8 maps se-  
 183 lected from the population (see below). The first has a set global average depth (SGAD)  
 184 whereas the second set had a set maximum depth (SMD). Both were computed by mul-  
 185 tiplying the grey-scale values with a constant. It was equal to 4500 for the SMD, so the  
 186 deepest point will be 4500m and the shallowest 900 m. The SGAD constant was indi-  
 187 vidually chosen so the mean depth of the ocean was 4500m. This gave a maximum depth  
 188 between 9500–42000m depending on the configuration. Depths of tens of kilometres, for  
 189 a planet of Earth's radius, is approaching the limit of the shallow-water approximation  
 190 employed in OTIS. The simulations are summarised in SM Table 1; note that the ex-  
 191 treme cases are not discussed further.

192 These 8 maps, with bathymetry, were also used to test the sensitivity to stratifi-  
 193 cation through simulations with enhanced ( $\gamma = 500$  in Eq. (4)) or reduced stratifica-  
 194 tion (using  $\gamma = 5$ ). The 8 maps, but with bathtub bathymetry, were also subject to tests  
 195 of the effect of the planet's rotation rate by adjusting Earth's day length to 3 hours and  
 196 8 days respectively, so that the new  $M_2$  periods are 1.51 and 124.20 hours. Only Earth's  
 197 rotation period is changed, no adjustment is made to the Lunar period of 27.3 days. Note  
 198 that a rotation period of 8 days still puts the planet within the fast-rotator regime of its  
 199 climate dynamics (Way et al., 2018).

## 200 2.2 Present Day Earth sensitivity simulations

201 Three simulations were run for present day Earth. The control used present day  
 202 ocean bathymetry, the first of two sensitivity simulations had a bathtub ocean with the  
 203 depth set to 4500m everywhere (see Fig. SM1a–b), whereas the second had Earths' shelf  
 204 seas removed by setting any ocean initially shallower than 1000m to 1800m to highlight  
 205 the importance of shelf dissipation. In the control, at the low resolution of  $1^\circ \times 1^\circ$ , OTIS  
 206 overestimates the  $M_2$  dissipation rate by a factor 2.5 compared to observed dissipation  
 207 rates [Egbert and Ray (2001); see our Fig. SM1], whereas  $S_2$  is overestimated by a fac-  
 208 tor 3. The bathtub configuration is far less dissipative (Fig. SM1b,c) and underestimates

209 the  $M_2$  and  $S_2$  dissipation rates by factors 25 and 200 respectively. Removing shelf seas  
 210 gives 0.77TW of  $M_2$  dissipation, compared to the 6.3TW of the control. These results  
 211 make sense dynamically. In a coarse-resolution simulation not enough energy dissipates  
 212 in the deep ocean due to underrepresented topography. Because the tidal energy is not  
 213 lost in the deep ocean, the shelf sea currents are overestimated and, with frictional losses  
 214 being proportional to the cube of the speed, the dissipation is overestimated. The same  
 215 happens in the bathtub runs, but there is then no shelf to dissipate the energy on, and  
 216 instead the global rate drops to deep abyssal values. The stratification sensitivity tests  
 217 can be found in the SM.

## 218 3 Results

### 219 3.1 Dissipation

220 As anticipated, the addition of continents of increasing complexity generates a more  
 221 energetic tide, highlighted for the eight examples in Fig. 1 and summarised in Fig. 2; these  
 222 are labelled A–H in the following and chosen because they cover the parameter space in  
 223 Fig. 2. The globally integrated dissipation in Fig. 2a scales with the magnitude of con-  
 224 tinental configuration complexity, quantified here as a ratio,  $R$ , between the coastline length  
 225 and the ocean basin area. As  $R$  increases, the  $M_2$  tidal dissipation rate follows and soon  
 226 reaches values two orders of magnitude larger than the rate in the equilibrium tide (i.e.,  
 227 the 2.3 GW at  $R = 0$ ). The dissipation range for a certain value of  $R$  can span nearly  
 228 an order of magnitude, but 36% of the configurations occur within the 0.1–1 TW range.  
 229 The  $S_2$  response is generally weak (not shown), with an amplitude of about 45% of  $M_2$ ,  
 230 although some configurations produce an  $S_2$  dissipation that is larger than  $M_2$  because  
 231 of  $S_2$  resonances, e.g., configuration E.

232 Both  $M_2$  and  $S_2$  reach dissipation maxima at continental distributions which are  
 233 qualitatively among the most fragmentary, with several small scale topographic features  
 234 introducing local flow acceleration. For  $M_2$ , the largest dissipation rate is 1.9 TW (Fig.  
 235 1E), while  $S_2$  peaks at 0.67 TW – values 19 and 260 times larger than in our bathtub  
 236 Earth simulation and on par with the observed dissipation rates on Earth today (Egbert  
 237 & Ray, 2001). As the coastline length continues to grow (i.e.,  $R$  increases), the conti-  
 238 nent area must also increase. This limits the total ocean area and therefore the poten-  
 239 tial for large integrated tidal dissipation rates as there is a smaller ocean to dissipate en-  
 240 ergy in. In the extreme case, we have a planet with a large number of basins too small  
 241 to host a tide. Thus, as  $R$  increases, we can expect dissipation to reduce, such as on a  
 242 surface with many disconnected basins, smaller than usual in our ensemble. This form  
 243 was not explicitly tested, but it would have quiescent tides under the conditions we use,  
 244 potentially expanding this range to a greater number of orders of magnitude. We leave  
 245 exploration of this limit to future work.

246 There is not a specific configuration, quantified by  $R$ , that is especially dissipative;  
 247 two configurations can have similar  $R$ -values, but be qualitatively dissimilar in the ac-  
 248 tual position of the landmasses (e.g., see configurations D and E in Fig. 1). Given that  
 249 global dissipation rates are dependent on oceanic area, a configuration that elevates dis-  
 250 sipation closer to the equator should result in a larger global value than one with a con-  
 251 tinent of the same shape at higher latitudes. However, a number of the simulations poss-  
 252 sess a polar ocean, e.g. H, or in some cases a single large hemispheric ocean with a large  
 253 tide. The dissipation in these instances can have a large deviation from what could be  
 254 expected, demonstrated in the increasing variability above very small  $R$ -values.

255 On present day Earth, deep ocean tidal dissipation is driven by conversion at bathy-  
 256 metric features (Egbert & Ray, 2001). The SMD configurations generally have an en-  
 257 hanced dissipation (see Figure 2b) influenced by the continental configuration. The two  
 258 sets – bathtub and SMD – are significantly different ( $F_{1,119} = 0.49$ ,  $p < 0.05$ ), with the

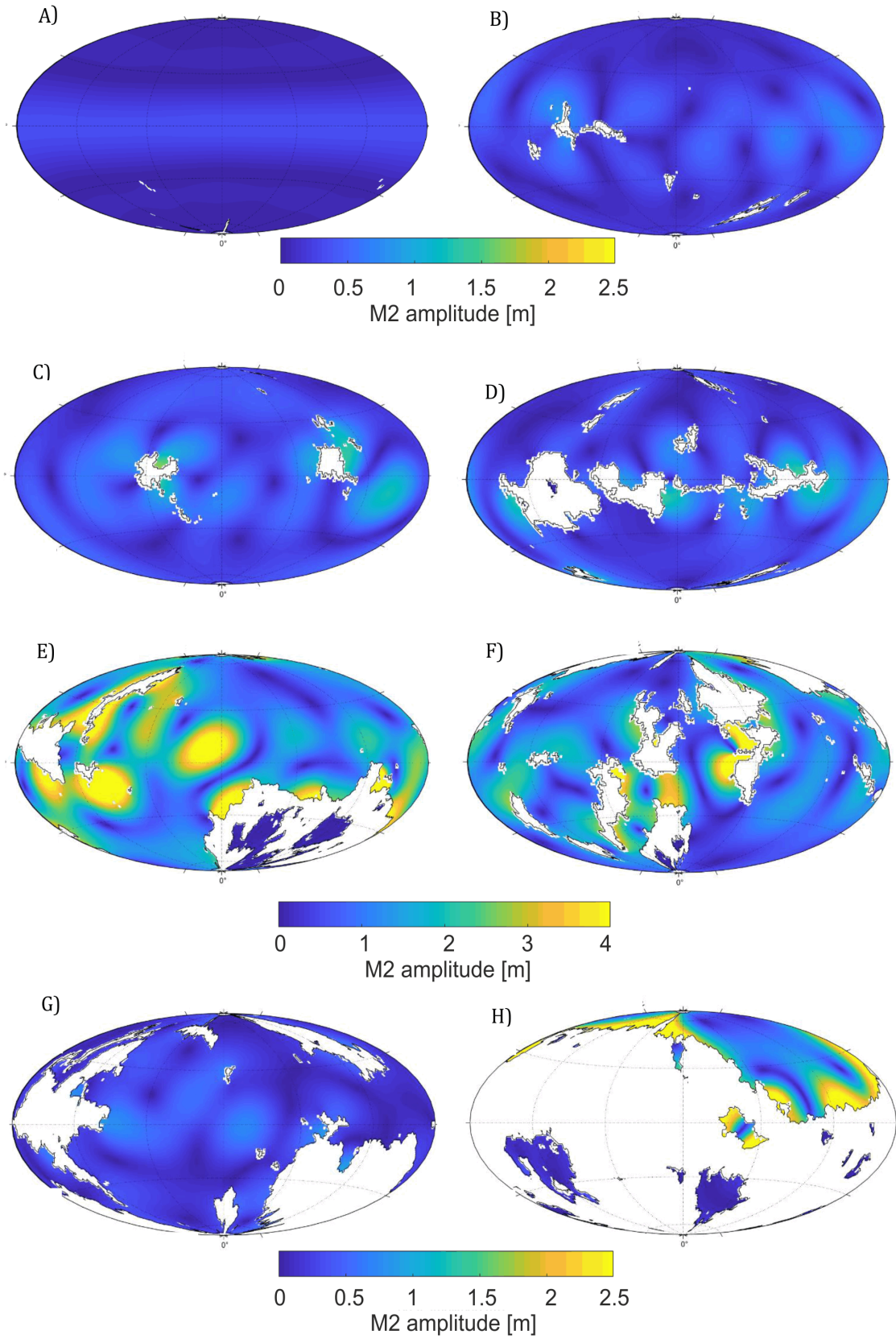


**Figure 1.**  $M_2$  Tidal amplitudes for the eight selected configurations, A–H. Note the use of two different colour scales: E and F use the second scale, whereas A–D and G–H use the first (which is repeated under panels G–H).



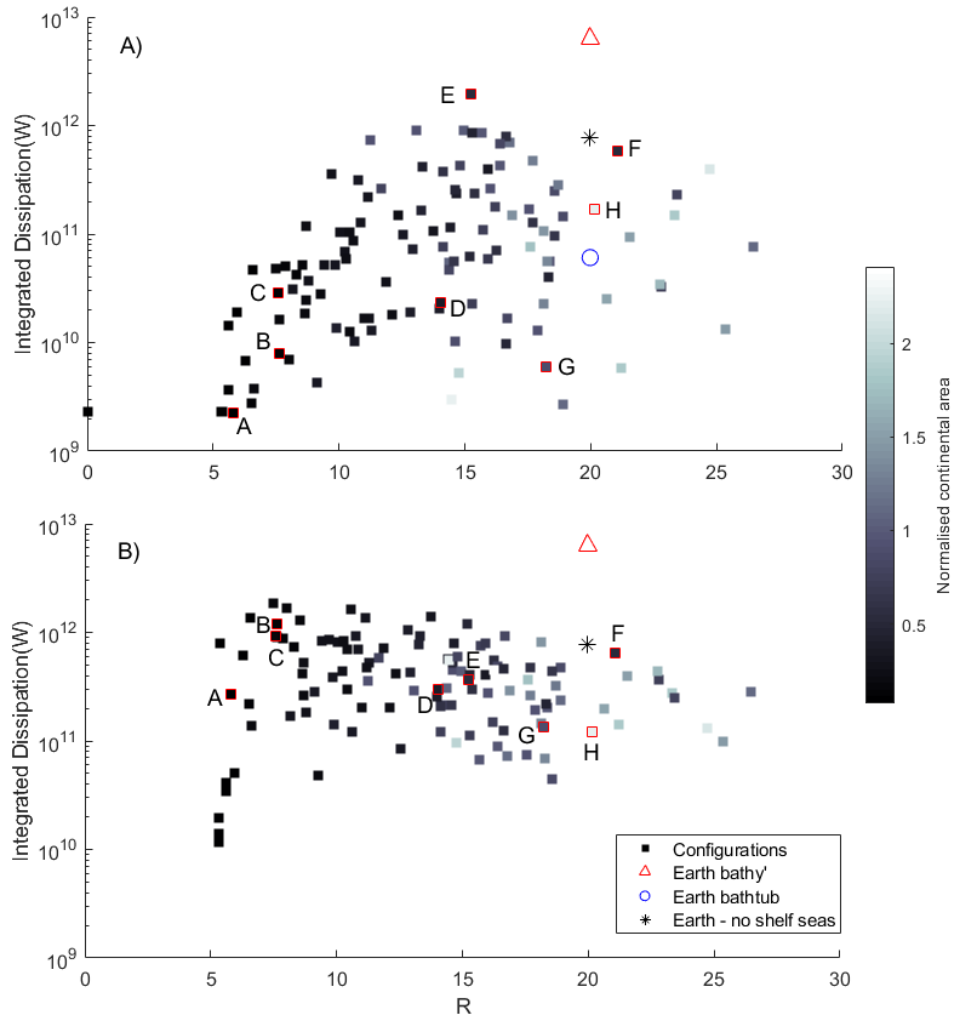


**Figure 2.** **A)**  $R$  versus the globally integrated dissipation rate,  $D$ . Note the selected 8 configurations, labelled A–H, outlined in red. The point at  $R=0$  is the control water-world, the Earth controls are shown as a circle (bathtub), triangle (with bathymetry), and the star is Earth without shelf seas. The colour scale of continent area has been normalised against Earth’s present continental area of  $5.1 \times 10^7 \text{ km}^2$ . Additional sensitivity simulations can be found in Table S1. Surfaces with some large number of small disconnected basins were not tested **B)** The same configurations, with a form of random bathymetry, Earth without shelf seas and the control are included for comparison.

259 bathtub dissipation values being poor predictors of the SMD values. The greatest increases  
 260 are amongst the configurations that were the least energetic without bathymetry, while  
 261 the bathtub maximum of 1.83TW can be achieved with smaller and less complex con-  
 262 tinents. Because our results span 3 orders of magnitude, any upper limit on Earth’s deep  
 263 ocean dissipation remains highly uncertain, however as our ensemble maxima are 1.83TW  
 264 and 1.92TW, such a limit may lie close to these values at this resolution. While the vari-  
 265 ance is large ( $s^2 = 7.24 \times 10^{10} \text{ TW}^2$ ), adding bathymetry narrows the range of dissi-  
 266 pation values compared to the runs without: 92% occur within one standard deviation  
 267 (0.39TW) of their mean (0.46TW) with bathymetry, as opposed to 76% without bathymetry,  
 268 although this still spans two orders of magnitude.

### 269 3.2 Sensitivity simulations

270 In the SGAD set, the dissipation rises three orders of magnitude at the lowest  $R$ -  
 271 value (see Table 1 SM). A consistent feature in these simulations is the convergence to-  
 272 wards a common dissipation value as the stratification is strengthened by a factor of 10:  
 273 the most energetic configurations are dampened whereas those at the scatter’s lower bound  
 274 are enhanced. In the SMD set, shown in Fig 2b, the trend is similar, however the dis-  
 275 sipation shows less variability within the  $R$  scale, while the examples lose their depen-  
 276 dence on  $R$ . The spatial distribution of the SMD runs are shown in Fig. 4 SM.

277 The planet’s rotation rate exerts a fundamental control on the tide (Green et al.,  
 278 2019) by setting resonant periods. Increasing Earth’s current rotation rate to 3 hours  
 279 also means the number of semi-diurnal periods in one present day Earth day rises from  
 280 2 to 8, thereby potentially increasing the energy dissipation over a certain fixed period  
 281 of time. This is indeed the case in the simulations herein, with dissipation enhanced in  
 282 each example, setting an upper bound on the scatter. The large increases for maps G  
 283 and F reflect the contribution of several smaller, resonant basins. With an 8 day day-  
 284 length, dissipation is reduced across all configurations. Crucially, the influence of con-  
 285 tinental configuration is still apparent, with the rotation adjustment conforming to the  
 286 upper and lower bounds of the scatter seen in Fig. 2a.

287 Our three frequency sensitivity simulations show, unsurprisingly, that dissipation  
 288 changes when the frequency is changed due to change in the resonant properties of the  
 289 basins. However, there is not necessarily a continuous trend in the results, nor can we  
 290 state if we have hit maximum global resonance in terms of rotation. For very fast or slow  
 291 spin rates resonances become more localised and will not contribute to globally integrated  
 292 dissipation rates to the same extent as at more moderate rates – see Green et al. (2019)  
 293 for a discussion.

### 294 3.3 An influence on the rotational evolution

295 The slowing of the planets rotation rate is tied to the magnitude of tidal dissipa-  
 296 tion. In Table 1 we give an estimate of the variability introduced in the day-length,  $\delta\text{LOD}$ ,  
 297 as a function of just the  $M_2$  frequency after  $10^6$  years. Eccentricity ( $e$ ) and obliquity are  
 298 0, and we make the assumption that  $de/dt = 0$ . From conservation of energy and mo-  
 299 mentum, for a small moon orbiting a rapidly rotating planet such as the Earth-Moon  
 300 system, the globally integrated dissipation,  $D$ , is related to the evolution of the Earth-  
 301 Moon separation,  $a$ , as:

$$D = \frac{1}{2}anM_M(\omega - n)\frac{da}{dt} \quad (5)$$

302 where  $M_M$  is the Moon’s mass ( $7.347 \times 10^{22} \text{ kg}$ ),  $\omega$  is the Earth’s angular rotation rate,  
 303  $a$  is the Earth-Moon separation,  $n = \sqrt{G(M_E + M_M)/a^3}$  is the mean motion of the Moon  
 304 ( $G = 6.674 \times 10^{-11} \text{ m}^3 \text{ kg}^{-1}\text{s}^{-2}$  is the gravitational constant and  $M_E = 5.972 \times 10^{24}$

**Table 1.** Shown are the bathtub and topographic example dissipation rates ( $D_{BT}$  and  $D_{BY}$ ) and the implications for the rotation rate,  $\delta LOD/Ma$  is the increase in day-length per  $10^6$  years relative to the present day-length.

Configuration	$D_{BT}$ (TW)	$D_{BY}$ (TW)	$\delta LOD_{BT}/Ma$ (s)	$\delta LOD_{BY}/Ma$ (s)
A	0.002	0.266	-0.013	-1.771
B	0.008	1.210	-0.053	-8.054
C	0.030	0.921	-0.200	-6.131
D	0.023	0.296	-0.153	-1.970
E	1.930	0.363	-12.847	-2.416
F	0.585	0.642	-3.894	-4.273
G	0.006	0.134	-0.040	-0.892
H	0.167	0.121	-1.112	-0.805

305 kg is Earth’s mass). The angular deceleration,  $d\omega/dt$ , is related to  $D$  as:

$$D = -I(\omega - n)\frac{d\omega}{dt} \quad (6)$$

306 in which  $I$  is the rotating Earth’s moment of inertia ( $8.04 \times 10^{37} \text{kg m}^{-2}$ ). An alterna-  
 307 tive method is given by MacDonald (1964). It is reasonable to assume that the values  
 308 computed here and shown in Table 1 are underestimated by up to an order of magni-  
 309 tude because of the relatively coarse resolution used in our model. An elevated dissipa-  
 310 tion of course leads to an increased  $\delta LOD$  and the linear dependence clearly shows the  
 311 importance of particular geologic features as the values in Table 1 do not consider shelf  
 312 seas. Alone, the real deep ocean dissipation (0.9TW) gives a  $\delta LOD$  of 5.1s from Eq. 6  
 313 over a million years, the total real integrated dissipation (3.6TW) gives 24s, or for just  
 314  $M_2$ , 16s. Our simulation without shelf seas slows by  $\sim 5$ s, compared to 42s for the full  
 315 bathymetry, illustrating the outsized effect of shallow water energy losses on the planet’s  
 316 rotational evolution.

## 317 4 Discussion

318 Continental configuration complexity matters in discussions of a planet’s tide be-  
 319 cause, for any given Earth-like planet, increasing the number of basins and/or embay-  
 320 ment type features will increase the probability of resonant amplification. Furthermore,  
 321 increasing the complexity of coastlines generates further energy loss due to acceleration  
 322 around peninsula-type features. Numerical simulations have been used to test the effect  
 323 of Earth’s former continental configurations and bathymetry on the tide (Bjerrum et al.,  
 324 2001; Green et al., 2017); however, to our knowledge there are no studies attempting to  
 325 test a general influence of continental complexity on the ocean tide. This is difficult to  
 326 do rigorously, given the problems in classifying complex non-Euclidean surfaces such as  
 327 realistic continents, shapes that were once described as ‘monstrosities’ (Mandelbrot, 1982).

328 Our results put a constraint on the rotational evolution of planets with oceans and  
 329 are of use for exoplanet estimates and deep time Earth tidal simulations alike. They also  
 330 highlight the fundamental effect topography has on ocean tides: even with a few small  
 331 continents or ocean bathymetry the dissipation can deviate by an order of magnitude  
 332 from the water world estimate. There is also a strong link between rotation rate and dis-  
 333 sipation (Green et al., 2019), and exoplanet rotation is currently difficult to determine  
 334 from observation. With an equilibrium tide, Kepler-22b (initial rotation period of 1 Day)  
 335 would have a rotation rate of about 2 Earth days after a 4.5Gyrs, while Proxima Cen-  
 336 tauri b (initial rotation period of 1 Day) would experience a rotation rate of some 12 days

337 (Barnes, 2017). We have shown that even with simple coastlines and a lack of bathymetry,  
 338 the spin down could vary with an order of magnitude, and be order(s) of magnitude larger  
 339 than in the equilibrium case.

340 As the continents aggregate and disperse during the 400–500Ma-long, super-continent  
 341 cycle (Matthews et al., 2016), the tides become anomalously energetic during periods  
 342 when the basins meet the conditions for resonance. A feature of this tectonically driven  
 343 super-tidal cycle (Green et al., 2018) is a much less energetic tide during super-continental  
 344 periods and a brief, more energetic state, for a few 10 Ma in between the subcontinents  
 345 (Gotlib & Kagan, 1985; Green et al., 2017). The trend for more complex configurations  
 346 to be more energetic in our results is analogous to this process and the tectonic setting  
 347 thus exerts a first order control on the tidal dissipation. For example, the basin config-  
 348 urations in Figure 2E and G are qualitatively similar, yet E is substantially more dis-  
 349 sipative due to its resonant state, whereas the large meridional continent in G blocks the  
 350 tide. Equally, the range of the dissipation scatter at any point along the complexity scale  
 351 ( $R$ ) is roughly an order of magnitude (see Fig. 2a), which is comparable to the super-  
 352 tidal fluctuation. Higher  $R$ -values tend to elevate dissipation, but not indefinitely. As  
 353 continent size increases, a threshold must be reached where ocean area declines and sup-  
 354 presses dissipation. This is a key geologic control on the rotational evolution (see Ta-  
 355 ble 1).

356 Earth’s earliest continental crust is considered to have mostly formed between 3–  
 357 2.5Ga (Korenaga, 2013, 2018), although this is debated. These early landmasses were  
 358 probably small (Goodwin, 1996; Scotese, 2004): estimates for the Late-Archean suggest  
 359 that  $\sim 12\%$  of Earth’s surface area was continental crust, with only 2–3% as emerged  
 360 land (Flament et al., 2008). This is compared to 42.5% of the surface being continen-  
 361 tal crust today, of which 27.5% is emerged land area (Schubert & Reymer, 1985; Fla-  
 362 ment et al., 2008; Cawood et al., 2013). In the micro-continental configurations in Fig 1A–  
 363 C, a small semi-diurnal tide would be expected, even with the shorter tidal period and  
 364 day-length at the time (Spalding & Fischer, 2019), but they still elevate the global dis-  
 365 sipation by nearly an order of magnitude above the equilibrium tide (Fig 2a). However,  
 366 this is still two orders of magnitude smaller than in simulations with larger, more nu-  
 367 merous landmasses that generate more complex basins. It is likely that while Earth had  
 368 a tidal dissipation rate much greater than the equilibrium tide early on in its history, it  
 369 may have become more energetic with the formation of larger continents. However this  
 370 result is not a model for an Archean tide; as shown, shelf-sea area and deep-ocean bathymetry,  
 371 both unknown for the period, would be key controls.

372 The amount of energy dissipated in our simulations suggests an upper limit near  
 373 1.9TW for the deep ocean dissipation, given the similarity between the simulations with  
 374 and without bathymetry. If the overestimation due to our coarse resolution is consid-  
 375 ered, a value of  $\sim 0.76$  TW may be more realistic, supported by the dissipation value pro-  
 376 duced without shelf seas (Fig 2). These values do of course depend upon the topographic  
 377 properties: even with a randomised bathymetry the influence of continental configura-  
 378 tion is clear, but is not necessarily a good predictor of the tidal dissipation. Also, the  
 379 smallest bathymetric features in our grids are of the order of  $\sim 100$  km horizontally, and  
 380 are of a higher relief than the Earth grid. Grid A for example possesses a canyon many  
 381 thousands of kilometres long. Given the nonlinear dependence on bathymetric slope in  
 382 Eq. 4), it is possible that the conversion fraction is overestimated, but this is an avenue  
 383 for future work.

384 The broader implication for Earth-like exoplanets is that while an ocean may raise  
 385 global tidal dissipation rates, a basin (or basins) with time-varying dimensions due to  
 386 tectonics will, in a similar fashion to Earth, cause this value to fluctuate considerably  
 387 over the planet’s history. We suggest that it could span three orders of magnitude solely  
 388 due to continental configuration. Planets with complex ocean bathymetry are likely to  
 389 have larger tidal dissipation rates, and hence spin down much quicker, than more bath-

390 tub like oceans. The apparent convergence generated by adding the SMD bathymetry  
 391 is an argument for including even a randomised ocean floor in planetary tidal models.

392 The tidal modulation by Earth’s tectonics gives these results a robust standard to  
 393 compare against, but the complexity metric may also have implications for Earth’s early  
 394 history, for periods with limited records of continental position and size.

### 395 Acknowledgments

396 Torben Morgensen’s advice on the use of the map generator is acknowledged. The sim-  
 397 ulations were done on Supercomputing Wales, and their support is greatly appreciated.  
 398 This work was supported by the NASA Astrobiology Program through collaborations  
 399 arising from our participation in the Nexus for Exoplanet System Science, and by the  
 400 NASA Planetary Atmospheres Program. RB acknowledges support from NASA grant  
 401 NNX15AN35G. MJW is thankful for support from the Goddard Space Flight Center’s  
 402 Sellers Exoplanet Environments Collaboration (SEEC), which is funded by the NASA  
 403 Planetary Science Division’s Internal Scientist Funding Model, and the NASA Habitable  
 404 Worlds Program. The data can be downloaded from the Open Science Framework (<https://osf.io/p7ay9/>).  
 405 Constructive comments from two anonymous reviewers greatly improved the manuscript.

### 406 References

- 407 Balbus, S. A. (2014). Dynamical, biological and anthropic consequences of equal lun-  
 408 nar and solar angular radii. *Proceedings of the Royal Society A: Mathematical,*  
 409 *Physical and Engineering Sciences*, 470(2168). doi: 10.1098/rspa.2014.0263
- 410 Barnes, R. (2017). Tidal locking of habitable exoplanets. *Celestial Mechanics and*  
 411 *Dynamical Astronomy*, 129(4), 509–536.
- 412 Batalha, N. M., Rowe, J. F., Bryson, S. T., Barclay, T., Burke, C. J., Caldwell,  
 413 D. A., . . . Welsh, W. F. (2013). Planetary candidates observed by kepler. III.  
 414 Analysis of the first 16 months of data. *Astrophysical Journal, Supplement*  
 415 *Series*, 204(2), 1–13. doi: 10.1088/0067-0049/204/2/24
- 416 Bills, B. G., & Ray, R. D. (1999). Lunar orbital evolution: A synthesis of recent re-  
 417 sults. *Geophysical Research Letters*, 26(19), 3045–3048.
- 418 Bjerrum, C. J., Surlyk, F., Callomon, J. H., & Slingerland, R. L. (2001). Numer-  
 419 ical paleoceanographic study of the early Jurassic transcontinental Laurasian  
 420 Seaway. *Paleoceanography*, 16(4), 390–404.
- 421 Boué, G., & Efroimsky, M. (2019, Jul). Tidal evolution of the Keplerian ele-  
 422 ments. *Celestial Mechanics and Dynamical Astronomy*, 131(7), 30. doi:  
 423 10.1007/s10569-019-9908-2
- 424 Cassan, A., Kubas, D., Beaulieu, J. P., Dominik, M., Horne, K., Greenhill, J.,  
 425 . . . Wyrzykowski, L. (2012). One or more bound planets per Milky Way  
 426 star from microlensing observations. *Nature*, 481(7380), 167–169. doi:  
 427 10.1038/nature10684
- 428 Cawood, P. A., Hawkesworth, C. J., Dhuime, B. (2013). The continental record and  
 429 the generation of continental crust. *GSA Bulletin*, 125(1-2), 14–32. doi: /10  
 430 .1130/B30722.1
- 431 Colose, C. M., Del Genio, A. D., & Way, M. J. (2019, May). Enhanced Habitabil-  
 432 ity on High Obliquity Bodies near the Outer Edge of the Habitable Zone of  
 433 Sun-like Stars. *arXiv e-prints*, arXiv:1905.09398.
- 434 Darwin, G. H. (1899). *The tides and kindred phenomena in the solar system*.  
 435 Houghton, Boston.
- 436 Dickey, J. O., Bender, P. L., Faller, J. E., Newhall, X. X., Ricklefs, R. L., Ries,  
 437 J. G., . . . Yoder, C. F. (1994, 7). Lunar Laser Ranging: A Continuing Legacy  
 438 of the Apollo Program. *Science*, 265(5171), 482 - 490.
- 439 Dressing, C. D., & Charbonneau, D. (2015). the Occurrence of Potentially Habitable  
 440 Planets Orbiting M Dwarfs Estimated From the Full Kepler Dataset and an

- 441 Empirical Measurement of the Detection Sensitivity. *Astrophysical Journal*,  
442 807(1), 45.
- 443 Dressing, C. D., Charbonneau, D., Dumusque, X., Gettel, S., Pepe, F., Col-  
444 lier Cameron, A., ... Watson, C. (2015). The mass of kepler-93b and the  
445 composition of terrestrial planets. *Astrophysical Journal*, 800(2).
- 446 Egbert, G. D., & Ray, R. D. (2001). Estimates of M2 tidal energy dissipation from  
447 TOPEX/Poseidon altimeter data. *Journal of Geophysical Research C: Oceans*,  
448 106(C10), 22475–22502. doi: 10.1029/2000JC000699
- 449 Egbert, G. D., Ray, R. D., & Bills, B. G. (2004). Numerical modeling of the global  
450 semidiurnal tide in the present day and in the last glacial maximum. *Journal*  
451 *of Geophysical Research: Oceans*, 109(C3).
- 452 Ferraz-Mello, S., Rodríguez, A., & Hussmann, H. (2008, May). Tidal friction in  
453 close-in satellites and exoplanets: The Darwin theory re-visited. *Celestial Me-*  
454 *chanics and Dynamical Astronomy*, 101, 171-201.
- 455 Flament, N., Coltice, N., & Rey, P. F. (2008). A case for late-Archaeon continen-  
456 tal emergence from thermal evolution models and hypsometry. *Earth and Plan-*  
457 *etary Science Letters*, 275(3-4), 326–336.
- 458 Fressin, F., Torres, G., Charbonneau, D., Bryson, S. T., Christiansen, J., Dressing,  
459 C. D., ... Batalha, N. M. (2013). The false positive rate of Kepler and the  
460 occurrence of planets. *Astrophysical Journal*, 766(2).
- 461 Goodchild, M. F., & Mark, D. M. (1987, 6). The Fractal Nature of Geographic Phen-  
462 omena. *Annals of the Association of American Geographers*, 77(2), 265–278.
- 463 Goodwin, A. M. (1996). *Principles of Precambrian geology* Elsevier.
- 464 Gotlib, V. Y., & Kagan, B. A. (1985). A reconstruction of the tides in the paleo-  
465 cean: Results of a numerical simulation. *Deutsche Hydrographische Zeitschrift*,  
466 38(2), 43–67.
- 467 Green, J., Way, M., & Barnes, R. (2019). Consequences of Tidal Dissipation in a  
468 Putative Venusian Ocean. *The Astrophysical Journal*, 876(2), L22.
- 469 Green, J. A. M., Huber, M., Waltham, D., Buzan, J., & Wells, M. (2017). Ex-  
470 plicitly modelled deep-time tidal dissipation and its implication for lu-  
471 nar history. *Earth and Planetary Science Letters*, 461, 46–53. doi:  
472 10.1016/j.epsl.2016.12.038
- 473 Green, J. A. M., Molloy, J. L., Davies, H. S., & Duarte, J. C. (2018). Is there a tec-  
474 tonically driven supertidal cycle? *Geophysical Research Letters*, 45, 3568–3576.  
475 doi: 10.1002/2017GL076695
- 476 Green, J. A. M., Way, M. J., & Barnes, R. (2019). Consequences of tidal dissipation  
477 in a putative venusian ocean. *The Astrophysical Journal Letters*, 876, 409-447.  
478 doi: 10.3847/2041-8213/ab133b
- 479 Hickman, A. E., Moore, C. M., Sharples, J., Lucas, M. I., Tilstone, G. H., Krivtsov,  
480 V., & Holligan, P. M. (2012). Primary production and nitrate uptake within  
481 the seasonal thermocline of a stratified shelf sea. *Marine Ecology Progress*  
482 *Series*, 463, 39–57. doi: 10.3354/meps09836
- 483 Howard, A. W. (2013). Observed properties of extrasolar planets. *Science*,  
484 340(6132), 572–576.
- 485 Kagan, B. (1997). Earth-Moon tidal evolution: Model results and observational evi-  
486 dence. *Progress in Oceanography*, 40(1-4), 109–124.
- 487 Kasting, J. F., Whitmire, D. P., & Reynolds, R. T. (1993). Habitable Zones around  
488 Main Sequence Stars. *Icarus*, 101(1), 108–128.
- 489 Kopparapu, R. K., Ramirez, R., Kasting, J. F., Eymet, V., Robinson, T. D., Ma-  
490 hadevan, S., ... Deshpande, R. (2013). Habitable zones around main-sequence  
491 stars: New estimates. *The Astrophysical Journal*, 765(2).
- 492 Korenaga, J. (2013). Initiation and evolution of plate tectonics on earth: Theories  
493 and observations. *The Annual Review of Earth and Planetary Sciences*, 41.
- 494 Korenaga, J. (2018). Estimating the formation age of distribution of continental  
495 crust by unmixing zircon ages. *Earth and Planetary Science Letters*, 482, 388–

- 496 395.
- 497 Kuhlbrodt, T., Griesel, A., Montoya, M., Levermann, A., & Rahmstorf, S. (2007).  
 498 On the driving processes of the atlantic meridional circulation. *Reviews of*  
 499 *Geophysics*, 45. doi: 10.1029/2004RG000166
- 500 Leconte, J., Chabrier, G., Baraffe, I., & Levrard, B. (2010, June). Is tidal heating  
 501 sufficient to explain bloated exoplanets? Consistent calculations accounting for  
 502 finite initial eccentricity. *Astro. & Astrophys.*, 516, A64+.
- 503 Lingam, M., & Loeb, A. (2018, 7). Implications of Tides for Life on Exoplanets. *As-*  
 504 *trobiology*, 18(7), 967–982.
- 505 MacDonald, G. J. F. (1964, 8). Tidal friction. *Reviews of Geophysics*, 2(3), 467–  
 506 541.
- 507 Mandelbrot, B. B. (1982). *The fractal geometry of nature* (Vol. 2). New York: WH  
 508 freeman New York.
- 509 Matthews, K. J., Maloney, K. T., Zahirovic, S., Williams, S. E., Seton, M., &  
 510 Muller, R. D. (2016). Global plate boundary evolution and kinematics since  
 511 the late Paleozoic. *Global and Planetary Change*, 146, 226–250.
- 512 Munk, W. (1968). Once again - tidal friction. *Quarterly Journal of the Royal Astro-*  
 513 *nomical Society*, 9(4), 352–375.
- 514 Munk, W. H. (1966). Abyssal recipes. *Deep-Sea Research and Oceanographic Ab-*  
 515 *stracts*, 13(4), 707–730.
- 516 Ray, R. D. (1997). Ocean self-attraction and loading in numerical tidal models. *Ma-*  
 517 *rine Geodesy*, 21, 181-192.
- 518 Ray, R. D., Eanes, R. J., & Chao, B. F. (1996). Detection of tidal dissipation in the  
 519 solid earth by satellite tracking and altimetry. *Nature*, 381, 595-597.
- 520 Renaud, J. P., & Henning, W. G. (2017). Increased Tidal Dissipation Using Ad-  
 521 vanced Rheological Models: Implications for Io and Tidally Active Exoplanets.  
 522 *The Astrophysical Journal*, 857(2), 98.
- 523 Schubert, G., & Reymer, A. P. S. (1985). Continental volume and freeboard through  
 524 geological time. *Nature*, 316(6026), 336–339.
- 525 Scotese, C. (2004). A Continental Drift Flipbook. *The Journal of Geology*, 112(6),  
 526 729–741.
- 527 Seager, S. (2013, 5). Exoplanet Habitability. *Science*, 340(6132), 577 LP - 581.
- 528 Simpson, J. H., Brown, J. G., Matthews, J., & Allen, G. (1990). Tidal straining,  
 529 density currents and stirring in the control of estuarine stratification. *Estuaries*  
 530 *and Coasts*, 13, 125-132. doi: 10.2307/1351581
- 531 Spalding, C., & Fischer, W. W. (2019). A shorter Archean day-length biases inter-  
 532 pretations of the early Earth’s climate. *Earth and Planetary Science Letters*,  
 533 514, 28–36.
- 534 Srokosz, M., Baringer, M., Bryden, H., Cunningham, S., Delworth, T., Lozier, S.,  
 535 ... Sutton, R. (2012, 3). Past, Present, and Future Changes in the Atlantic  
 536 Meridional Overturning Circulation. *Bulletin of the American Meteorological*  
 537 *Society*, 93(11), 1663–1676.
- 538 Stammer, D., Ray, R. D., Andersen, O. B., Arbic, B. K., Bosch, W., Carrère, L., ...  
 539 Yi, Y. (2014). Accuracy assessment of global barotropic ocean tide models.  
 540 *Reviews of Geophysics*, 52(3), 243–282.
- 541 Taylor, G. I. (1920). Tidal friction in the irish sea. *Proceedings of the Royal Society*  
 542 *of London series A*, 96, doi: 10.1098/rspa.1919.0059.
- 543 Tsiaras, A., Waldmann, I. P., Tinetti, G., Tennyson, J., & Yurchenko, S. N. (2019).  
 544 Water vapour in the atmosphere of the habitable-zone eight-earth-mass planet  
 545 k2-18 b. *Nature Astronomy*. doi: 10.1038/s41550-019-0878-9
- 546 Tuerena, R. E., Williams, R. G., Mahaffey, C., Vic, C., Green, J. A. M., Naveira-  
 547 Garabato, A., ... Sharples, J. (2019). Internal tides drive nutrient fluxes into  
 548 the deep chlorophyll maximum over mid-ocean ridges. *Global Biogeochemical*  
 549 *Cycles*, 33, 995-1009.
- 550 Way, M. J., Del Genio, A. D., Aleinov, I., Clune, T. L., Robinson, T. D., Kelly, M.,

- 551 & Kiang, N. Y. (2018). Climates of warm earth-like planets. i. 3d model  
552 simulations. *The Astrophysical Journal Supplement Series*, 239(2).
- 553 Way, M. J., Genio, A. D. D., Kiang, N. Y., Sohl, L. E., Grinspoon, D. H., Aleinov,  
554 I., ... Al, W. A. Y. E. T. (2016). Was Venus the first habitable world of our  
555 solar system? *Geophysical Research Letters*, 43, 8376-8383.
- 556 Way, M. J., & Georgakarakos, N. (2017, Jan). Effects of Variable Eccentricity on the  
557 Climate of an Earth-like World. *Astrophysical Journal Letters*, 835(1), L1. doi:  
558 10.3847/2041-8213/835/1/L1
- 559 Way, M. J., & Del Genio, N. (2019, Dec). Venusian Habitable Climate Sce-  
560 narios: Modeling Venus through time and applications to slowly rotating  
561 Venus-Like Exoplanets. *Journal of Geophysical Research: Planets*. doi:  
562 10.1029/2019JE006276
- 563 Williams, D. M., & Pollard, D. (2002, Jan). Earth-like worlds on eccentric orbits:  
564 excursions beyond the habitable zone. *International Journal of Astrobiology*,  
565 1, 61-69. doi: 10.1017/S1473550402001064
- 566 Williams, D. M., & Pollard, D. (2003, Jan). Extraordinary climates of Earth-like  
567 planets: three-dimensional climate simulations at extreme obliquity. *Interna-  
568 tional Journal of Astrobiology*, 2(1), 1-19. doi: 10.1017/S1473550403001356
- 569 Williams, G. J., Sandin, S. A., Zgliczynski, B. J., Fox, M. D., Gove, J. M., Rogers,  
570 J. S., ... Smith, J. E. (2018). Biophysical drivers of coral trophic depth  
571 zonation. *Marine Biology*, 165(4), 60.
- 572 Williams, J. G., Sinclair, W. S., & Yoder, C. F. (1978). Tidal acceleration of the  
573 moon. *Geophysical Research Letters*, 5(11). doi: 10.1029/GL005i011p00943
- 574 Wilmes, S.-B., Green, J. A. M., Gomez, N., Rippeth, T. P., & Lau, H. (2017).  
575 Global Tidal Impacts of Large-Scale Ice-Sheet Collapses. *Journal of Geophysi-  
576 cal Research: Oceans*, 1-17.
- 577 Wunsch, C., & Ferrari, R. (2004). Vertical mixing, energy, and the general circula-  
578 tion of the oceans. *Annual Review of Fluid Mechanics*, 36(1), 281-314.
- 579 Yang, J., Boué, G., Fabrycky, D. C., & Abbot, D. S. (2014). Strong dependence of  
580 the inner edge of the habitable zone on planetary rotation rate. *Astrophysical  
581 Journal Letters*, 787(1).
- 582 Zaron, E. D., & Egbert, G. D. (2006). Estimating Open-Ocean Barotropic Tidal  
583 Dissipation: The Hawaiian Ridge. *Journal of Physical Oceanography*, 36(6),  
584 1019-1035.